GEOPHYSICAL RESEARCH LETTERS, VOL. 27, NO. 8, PAGES 1103-1106, APRIL 15, 2000

Estimation of the aerosol perturbation to the Earth's radiative budget over oceans using POLDER satellite aerosol retrievals

O. Boucher and D. Tanré

LOA, Université des Sciences et Technologies de Lille, Villeneuve d'Ascq, France

Abstract. POLDER satellite retrievals of aerosol properties over oceans are used to estimate a global-mean clear-sky aerosol shortwave flux perturbation of order -5 to -6 Wm^{-2}. Uncertainties due to aerosol absorption and POLDER cloud screening algorithm are quantified. In order to bound the radiative forcing by anthropogenic aerosols, we attempt to remove the contribution of background aerosols from these estimates and present all-sky aerosol radiative effects for three regions and two methods. The results are sensitive to the thresholds used to define the background conditions.

1. Introduction

Aerosols influence the radiative balance of the Earth through scattering of radiation (the direct effect) and by modifying the microphysical and optical properties of clouds (the indirect effect). Estimates of the aerosol direct effect and aerosol direct radiative forcing (defined as the anthropogenic fraction of the aerosol direct effect) are largely based on models. Aircraft observations [*Hignett et al.*, 1999] confirm that aerosols cause a significant modification in the clear-sky radiative budget. *Haywood et al.* [1999] have shown that model-based aerosol distributions could explain a large part of the discrepancies between ERBE satellite-observed and model-simulated clear-sky albedos. *Bergstrom and Russell* [1999] estimated the direct aerosol effect over the mid-latitude North Atlantic Ocean by combining AVHRR measurements of aerosol optical depth to in-situ measurements of aerosol physical properties obtained during the TARFOX campaign. Improved algorithms applied to AVHRR [*Nakajima and Higurashi*, 1998] or POLDER (Polarization and Directionality of the Earth's Reflectances, *Deuzé et al.* [1999]) radiometers now make it possible to retrieve the aerosol Ångström coefficient. In this paper, we use the POLDER retrieved aerosol properties to estimate the global-scale aerosol impact on the Earth's radiative budget.

2. Aerosol radiative perturbation

2.1. Description of POLDER aerosol products

We limit our analysis to oceanic regions. The aerosol products consist of the aerosol optical thickness (at 865 nm), aerosol Ångström coefficient (computed between the 670 and 865 nm channels) [*Deuzé et al.*, 1999]. The spatial resolution for the level-2 data is about 20 km x 20 km. The aerosol retrieval is based on a look-up table (LUT) approach including 12 different aerosol models using 3 different representative refractive indices (Table 1). The aerosol optical depth and Ångström coefficient are adjusted in order to obtain the best fit to the observed radiances at 670 and 865 nm. For Ångström coefficient below -0.2, which are usually associated to low aerosol optical depths, aerosol model #5 in Table 1 is used. Note finally that the cloud screening is quite stringent in its present version.

Paper number 1999GL010963.
0094-8276/00/1999GL010963$05.00

2.2. Computation of aerosol flux perturbation

We first construct a look-up table of the aerosol-induced top-of-atmosphere flux change for each of the 12 aerosol models of Table 1 and for 10 values of the solar zenith angle. Since it was shown in *Boucher et al.* [1998] that the aerosol forcing was to a good approximation proportional to $(1 - e^{-\tau})$, we only compute the aerosol radiative perturbation for an aerosol optical depth τ_0=0.1 at 865 nm. We use the Streamer radiative code [*Key*, 1994] which compares well with more elaborated codes [*Boucher et al.*, 1998]. For all seasons, we use a mid-latitude summer profile. Use of different profiles makes very small (at most 5%) differences. We also assume that the aerosol layer is located below 2 km. The surface reflectance is that of the open ocean and includes variation with solar zenith angle, although it is assumed to be Lambertian. For the calculations of the surface reflectance due to the presence of foam and the effect of waves on the Fresnel reflection, the 10-m wind speed is taken constant at 10 ms^{-1}.

Fig. 1 shows the aerosol perturbation to the radiative budget as a function of the solar zenith angle for a constant

Table 1. Description of aerosol models used in this study. Columns 2–4 correspond to the aerosol models used in the POLDER retrieval and in our calculation of aerosol-induced flux change. Columns 5–7 correspond to the modified models used for sensitivity tests (see text). For computing the Mie scattering properties, log-normal size distributions are used with geometric standard deviation, σ_g=2.37. The aerosol refractive index is assumed constant over the solar spectrum.

Aerosol Model	Aerosol Modal Radius (μm)	Refractive Index	α	Modified Refractive Index	Modified Aerosol Radius (μm)	SSA at 550 nm
1	0.2710	$1.33-0.0i$	0.0	$1.33-0.01i$	0.2119	.832
2	0.1445	$1.33-0.0i$	0.3	$1.33-0.01i$	0.1308	.874
3	0.0713	$1.33-0.0i$	0.8	$1.33-0.01i$	0.0678	.907
4	0.0335	$1.33-0.0i$	1.4	$1.33-0.01i$	0.0324	.916
5	0.2239	$1.40-0.0i$	0.0	$1.40-0.01i$	0.1805	.846
6	0.1216	$1.40-0.0i$	0.3	$1.40-0.01i$	0.1116	.886
7	0.0602	$1.40-0.0i$	0.8	$1.40-0.01i$	0.0584	.916
8	0.0293	$1.40-0.0i$	1.4	$1.40-0.01i$	0.0285	.926
9	0.1815	$1.50-0.0i$	0.0	$1.50-0.01i$	0.1485	.859
10	0.1000	$1.50-0.0i$	0.3	$1.50-0.01i$	0.0921	.896
11	0.05096	$1.50-0.0i$	0.8	$1.50-0.01i$	0.0489	.924
12	0.02520	$1.50-0.0i$	1.4	$1.50-0.01i$	0.0246	.935

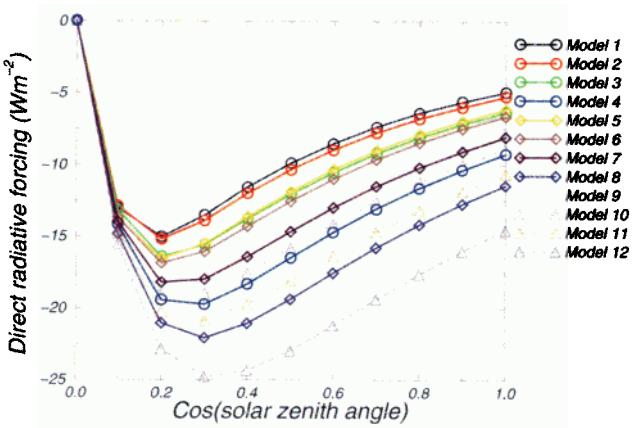

Figure 1. Change in solar radiative flux at the top-of-atmosphere due to aerosols as function of the cosine of the solar zenith angle. The data are for an aerosol optical depth of 0.1 at 865 nm and for the 12 aerosol models from Table 1. The aerosol models for the dashed curves are hardly used by the algorithm.

aerosol optical depth of 0.1 at 865 nm. We recognize on Fig. 1 the conventional maximum in aerosol radiative effect for scattering angles of about 60° [*Boucher et al.*, 1998]. This maximum is somewhat reduced because of the increase in surface reflectance with solar zenith angle [*Russell et al.*, 1997].

For computing the aerosol perturbation pixel-by-pixel, the values of aerosol-induced flux change of the LUT are interpolated in solar zenith angle and aerosol Ångström coefficient, but not in aerosol refractive index, which only takes the 3 values of Table 1. For each pixel i, the daily-averaged aerosol perturbation at the top-of-atmosphere is then approximated as:

$$\Delta F_i = \int_{\text{day}} \Delta F(\tau_0, \alpha_i, m_i, \mu_i(t)) \frac{1-e^{-\tau_i}}{1-e^{-\tau_0}} dt \; / \int_{\text{day}} dt \quad (1)$$

where $\mu_i(t)$ is the cosine of the solar zenith angle at time of the day t; τ_i, α_i, and m_i are the measured aerosol optical depth, Ångström coefficient, and refractive index at pixel i. It is implicit in Equation (1) that the one-time daily observation of POLDER (10.30 local time at the Equator) is representative of daytime values.

2.3. Results

Fig. 2 shows the change in clear-sky top-of-atmosphere solar radiative flux for the aerosol distribution retrieved by POLDER for December 1996 and June 1997. These maps resemble maps of the monthly-mean aerosol optical depth showed in *Deuzé et al.* [1999], except for that the aerosol radiative effect is enhanced in regions of high Ångström coefficient. It should be made clear that the POLDER clear-sky conditions are different –and may not be representative– of the actual clear-sky conditions, especially in regions of fractional cloudiness. This may result in an underprediction of the radiative impact of secondary aerosols which are partly produced through in-cloud processes. We displayed the global and hemispheric means of the aerosol direct effect in Fig. 3. The global mean is relatively constant at -5 to -6 Wm^{-2}. The mean is larger in the northern hemisphere than in the southern hemisphere by 1 to 3 Wm^{-2}, depending on the season. These numbers fall in the range of the model-based estimates of the clear-sky aerosol effect given by *Haywood et al.* [1999] assuming low and high sea-salt burdens.

3. Discussion of uncertainties

There are various sources of uncertainties in our estimates. These can be due to uncertainties in the retrieved aerosol properties, or in the aerosol vertical profile, spectral refractive index, and sea surface albedo used for the flux calculations. The uncertainties that are most easily quantifiable are discussed below.

3.1. Influence of aerosol absorption

The aerosol models used in the POLDER algorithm (Table 1, columns 1–4) are non-absorbing in the solar spectrum. We have introduced some absorption by setting the imaginary index to $-0.01i$ throughout the solar spectrum. The aerosol models are modified in such a way that the Ångström coefficients for scattering remain the same (Table 1, columns 5–7). This results in aerosol single scattering albedo at 550 nm ranging from 0.83 to 0.94 depending on the model. The aerosol flux perturbation is then computed for the new aerosol radiative properties in the same way as before, except that the measured aerosol optical depth is increased by a factor equal to one over the aerosol single scattering albedo at 865 nm, ω. This accounts for the fact that, at first order, the aerosol contribution to the observed radiance is proportional to the product $\omega\,\tau$. For a constant $\omega\,\tau$, the flux change induced by absorbing aerosols is smaller than induced by non-absorbing aerosols by 10 to 20% and 20 to 70% for large and small solar zenith angles, respectively. The reason for this decrease is in enhanced absorption due to multiple scattering effects within the aerosol layer and

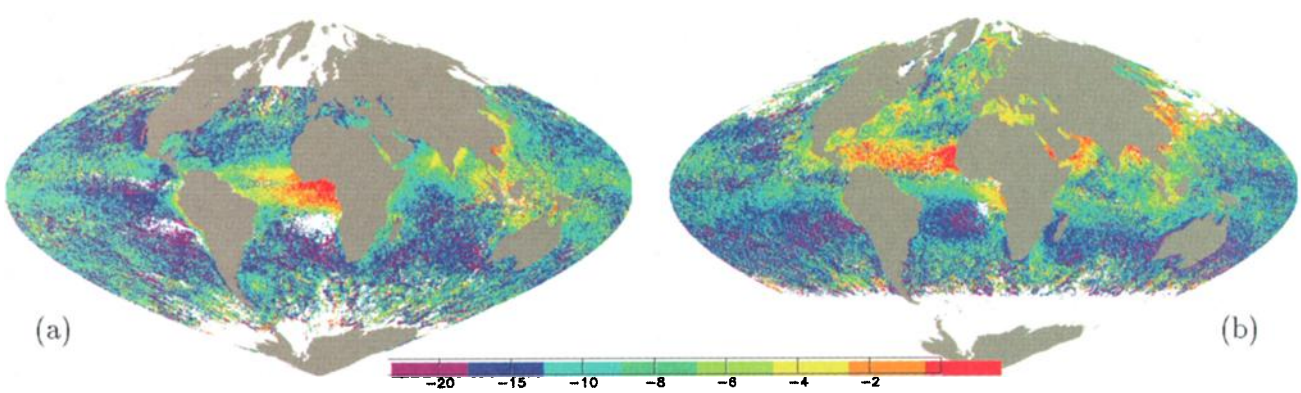

Figure 2. Clear-sky shortwave aerosol radiative perturbation (Wm^{-2}) computed from the POLDER aerosol retrievals for a) December 1996 and b) June 1997.

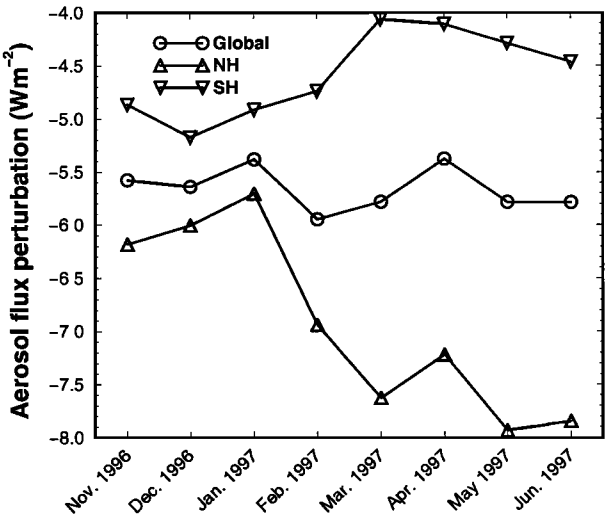

Figure 3. Global and hemispheric means in clear-sky aerosol radiative perturbation (Wm^{-2}).

between the sea surface and the aerosol layer. Globally averaged, the aerosol flux perturbation is decreased by 32% upon inclusion of aerosol absorption. We think that this represents an upper limit for the effect of aerosol absorption.

3.2. Influence of POLDER cloud screening

By eliminating aerosol optical depth larger than about 0.8, the present cloud screening tends to bias the retrieval towards smaller values of aerosol optical depth. The aerosol retrieval in June 1997 was reprocessed with a less stringent cloud screening. This results in a 34% increase in the aerosol-induced flux change for June 1997. The bulk of the increase comes from the Atlantic Ocean where optical depths for dust aerosol are significantly increased. This 34% increase in flux change should nevertheless be seen as an upper bound since it may also incorporate pixels contaminated by clouds.

3.3. Influence of aerosol Ångström coefficient

Goloub et al. [1999] showed that the POLDER aerosol optical depth was in good agreement with surface-based sun-photometer measurements ($\pm 0.05 \pm 0.05\ \tau$, with no bias observed). However the aerosol Ångström coefficient was underpredicted for aerosol optical depths larger than 0.1. Globally-averaged, a 10% underestimation in the Ångström coefficient results into a 1% underestimation of the aerosol-induced flux change.

3.4. Influence of geometric standard deviation

The geometric standard deviation, σ_g, is fixed at 2.37 in the aerosol retrieval scheme. We conducted a sensitivity test where σ_g is taken equal to 2.0 and 2.7 in the flux calculations. As for the test on absorption, the aerosol modal radii are modified as to keep the Ångström coefficient to the same reference values. Such modifications have a negligible influence on our results.

However, the use of bimodal aerosol models, in contrast to the monomodal aerosol models of the present retrieval scheme, could lead to differences in the retrieved aerosol properties. It is not yet possible to quantify the subsequent uncertainty in aerosol flux change.

4. Towards estimating aerosol forcing

4.1. Method

The perturbation to the Earth's radiative budget computed in the previous section includes the effects of both natural and anthropogenic aerosols, the relative contributions of which are difficult to determine in the context of present satellite (and in-situ) measurements. In order to place an upper bound on the aerosol radiative forcing, we attempt to define a "background" (or natural) aerosol level and substract its radiative effect from the total aerosol radia-

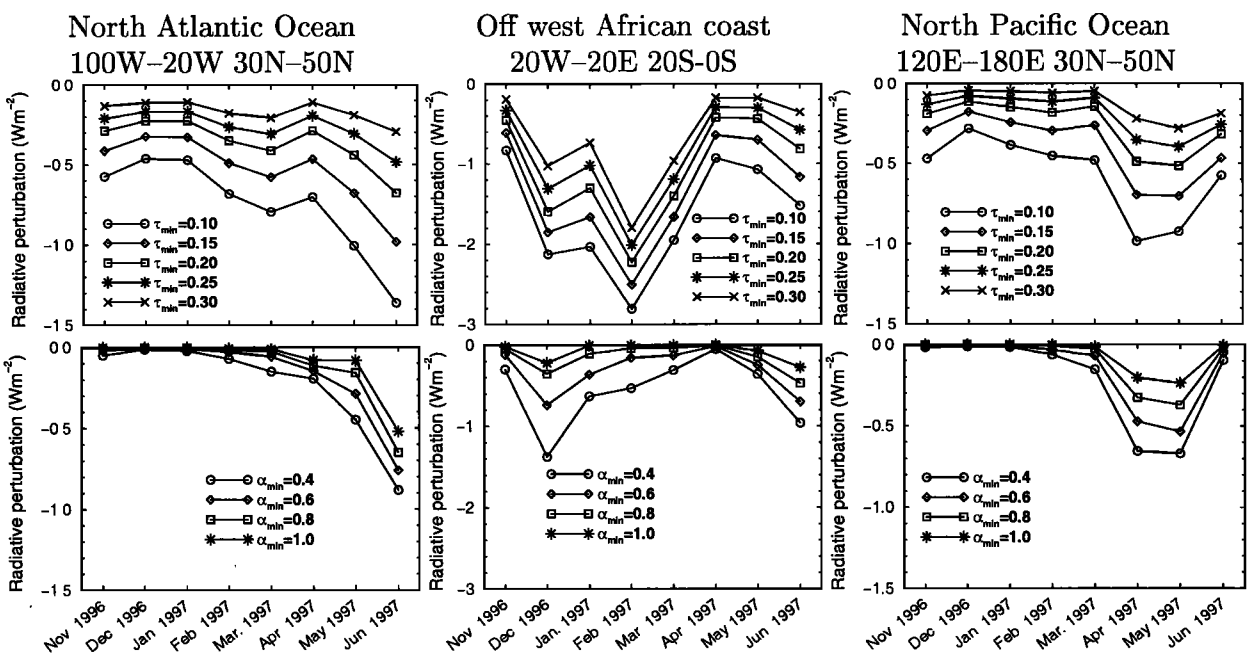

Figure 4. Seasonal variation in all-sky aerosol radiative effect (Wm^{-2}) over the North Atlantic, off the west African coast, and over the North Pacific for methods A (upper panels) and B ($\tau_{\min}$=0.10, lower panels).

tive effect. For this, we compute a clear-sky aerosol radiative perturbation as

$$\Delta RF_{\text{clear}} = \sum_{i \notin \text{bg}} (\Delta F_i - \overline{\Delta F_{\text{bg}}})/N \qquad (2)$$

where N is the number of equal-area pixels in the region under consideration, $\overline{\Delta F_{\text{bg}}}$ is the average radiative perturbation over the background pixels, while i runs over the remaining pixels.

The all-sky radiative effect is computed as the product of the clear-sky effect by the fraction of clear sky as given by the cloud processing line of the POLDER algorithm [*Buriez et al.*, 1997]. By so doing, we assume (i) that the fraction of clear sky where the aerosol retrieval is performed is representative of the total clear sky, and (ii) that the the cloudy-sky part of the direct aerosol effect is negligible, which is still under debate.

In method A the background encompasses all the pixels where the aerosol optical depth is smaller than a threshold, so that $\overline{\Delta F_{\text{bg}}} = \overline{\Delta F_{\tau<\tau_{\min}}}$. In method B, the background is defined as in method A but the summation in Eq. 2 is restricted to pixels for which both τ and α are larger than the thresholds $\tau_{\min}$ and $\alpha_{\min}$. While method A assumes that anthropogenic effects can be bounded by considering only the largest aerosol optical depths, method B also implies that only small particles are of anthropogenic origin. Since some large aerosols, such as Saharan dust, may be of anthropogenic origin, the actual aerosol radiative forcing may lie somewhere between the estimates given by methods A and B.

4.2. Results

The all-sky radiative effects are considerably reduced compared to their clear-sky counterparts. For illustration, we plot in Fig. 4 the seasonal (i.e., 8 month) variation in aerosol all-sky radiative effect for three regions. As expected, aerosol radiative effects estimated from method B are smaller than from method A. Their temporal variation may also be different, which indicates a seasonal evolution in the aerosol properties.

Over the North Atlantic Ocean (30N-50N), the aerosol effect as computed by method A includes an important contribution by mineral dust particles through November to April. The anthropogenic origin of this dust is however not established. In May and June, the effect is rather due to small aerosol particles coming from the United States, as evidenced by the larger effect predicted by method B. Off west African coast (20S-0S), large radiative effects are found in December 1996 and June 1997 according to method B, which are probably due to biomass burning. It is intriguing that the large peak observed in February in method A is absent in method B. It may be due to dust transported from arid regions or aged particles coming from biomass burning and transported over long distances. Over the North Pacific Ocean (30N–50N), the effect is maximum in April–May 1997, when aerosols with high Ångström coefficients are observed.

The choice of the threshold aerosol optical depth and Ångström coefficient remains open. The background maritime conditions corresponds to POLDER aerosol optical depth of the order of 0.1 and Ångström coefficient close to 0. Ångström coefficients larger than 0.4 are only found close to the continents, which could indicate an anthropogenic origin. Sunphotometer measurements suggest, however, larger Ångström coefficients for industrial aerosols. This and the large sensitivity of the aerosol effect to the threshold Ångström coefficient prevent us from a definitive conclusion.

5. Conclusions

We estimated the shortwave radiative flux change due to aerosols from the POLDER satellite retrievals. Our results show that the clear-sky shortwave radiative perturbation amounts to about -5.5 Wm^{-2}, globally-averaged, with significant uncertainties due to aerosol absorption and choice of the POLDER cloud screening method. We further attempted to remove the contribution of background aerosols from the estimates given above in order to bound the radiative forcing by anthropogenic aerosols. This was done by applying thresholds on the aerosol optical depth and Ångström coefficient. It turned out that the estimated radiative effects vary considerably depending on the choice of these thresholds. A research effort is needed to identify aerosol types and the anthropogenic fraction of the aerosol burden from remote and in-situ measurements.

Acknowledgments. Aurélia Marchand is acknowledged for her help in processing the POLDER data. POLDER is a joint CNES/NASDA effort. Information on the POLDER products can be found at http://polder@www-projet.cnes.fr:8060/ We thank two reviewers for their constructive comments.

References

Bergstrom, R. W., and P. B. Russell, Estimation of aerosol direct radiative effects over the midlatitude North Atlantic from satellite and in situ measurements, *Geophys. Res. Lett.*, *26*, 1731–1734, 1999.

Boucher, O., et al., Intercomparison of models representing shortwave radiative forcing by sulfate aerosols, *J. Geophys. Res.*, *103*, 16,979–16,998, 1998.

Buriez, J.-C, C. Vanbauce, F. Parol, P. Goloub, M. Herman, B. Bonnel, Y. Fouquart, P. Couvert, and G. Sèze, Cloud detection and derivation of cloud properties from POLDER, *Int. J. Remote Sensing*, *18*, 2785–2813, 1997.

Deuzé, J.-L., M. Herman, P. Goloub, and D. Tanré, Characterization of aerosols over ocean from POLDER/ADEOS-1, *Geophys. Res. Lett.*, *26*, 1421–1424, 1999.

Goloub, P., D. Tanré, J.-L. Deuzé, M. Herman, A. Marchand, and F.-M. Bréon, Validation of the first algorithm applied for deriving the aerosol properties over the ocean using the POLDER/ADEOS measurements, *IEEE Trans. Geosc. Rem. Sens.*, *37*, 1586–1596, 1999.

Haywood, J. M., V. Ramaswamy, and B. J. Soden, Tropospheric aerosol climate forcing in clear-sky satellite observations over the oceans, *Science*, *283*, 1299–1303, 1999.

Hignett, P., J. P. Taylor, P. N. Francis, and M. D. Glew, Comparison of observed and modeled direct aerosol forcing during TARFOX, *J. Geophys. Res.*, *104*, 2279–2287, 1999.

Key, J., *Streamer user's guide*, Coop. Inst. Res. Environ. Sci., University of Colorado, 71 pp., 1994.

Nakajima, T., and A. Higurashi, A use of two-channel radiances for an aerosol characterization from space, *Geophys. Res. Lett.*, *25*, 3815–3818, 1998.

Russell, P. B., S. A. Kinne, and R. W. Bergstrom, Aerosol climate effects: Local radiative forcing and column closure experiments, *J. Geophys. Res.*, *102*, 9397–9407, 1997.

O. Boucher and D. Tanré, Laboratoire d'Optique Atmosphérique, Bât. P5, Université des Sciences et Technologies de Lille, 59655 Villeneuve d'Ascq Cedex, France. (e-mail: boucher@loa.univ-lille1.fr, tanre@loa.univ-lille1.fr)

(Received July 28, 1999; revised November 9, 1999; accepted January 6, 2000.)